

# Pinned and bound modes of charge density wave type collective excitation in $\text{SmNiO}_3$ as revealed by terahertz spectroscopy

Sarmistha Das , G. L. Prajapati, and D. S. Rana \**Department of Physics, Indian Institute of Science Education and Research Bhopal, Madhya Pradesh 462066, India*

(Received 8 October 2020; accepted 13 November 2020; published 2 December 2020)

The terahertz (THz) optical conductivity of charge-ordered nickelate  $\text{SmNiO}_3$  thin films depicts a unique dependence of the charge-density-wave (CDW) type instability on the film thickness. Here, we report a rare observation of two dominant resonance modes in the THz conductivity spectrum. Corroborated by structural and electrical conductivity data, we demonstrate that these doublet excitations are the attribution of the CDW type pinned and bound modes. Both the peak position and the peak strength can be controlled by the film thickness and the defect density associated with oxygen stoichiometry. The oxygen vacancies in these films act like defects/impurities and induce charge oscillation around them which get coupled with unperturbed CDW mode of the charge-ordered phase. Thus, an additional bound mode emerges alongside the pinned mode. The defect density as controlled by the film thickness allows modulation of the resonance excitations in the desired THz frequency range.

DOI: [10.1103/PhysRevB.102.214403](https://doi.org/10.1103/PhysRevB.102.214403)

## I. INTRODUCTION

Many nontrivial effects, emerging at the crossover of the localized to itinerant electronic ground state comprising unstable and partially occupied degenerate levels, enrich the recent research in perovskite rare-earth nickelates ( $\text{RNiO}_3$ ) [1–5]. Unravelling the complex ordering phenomena in the low temperature insulating ground state of these nickelates offers a unique platform for studying subtle intricacies associated with the competing energetics of charge, spin, lattice, and orbitals. The temperature driven metal to insulator transition (MIT) is one such property in which the evolution of the insulating ground state as a function of cation size is a result of competing energetics. For heavy rare-earth ions, the MIT temperature ( $T_{\text{MI}}$ ) increases, accompanied by a symmetry lowering transition with more distorted unit cell structure. Thus, transition is further governed by a complex mechanism which involves the symmetry breaking monoclinic distortion and associated rearrangement of Ni positions in the crystal array [1–5].

The ground state of such MIT is quite diverse in nature, accompanying different forms of spin, charge, and orbital order [2,6–9]. Some recent theoretical and experimental studies have revealed that the insulating state is associated with the  $\text{Ni}^{3+\delta}$  and  $\text{Ni}^{3-\delta}$  charge disproportionated and charge-ordered (CO) state. Therefore, a charge density wave (CDW) type instability is expected to manifest due to the distortion of alternative  $\text{NiO}_6$  octahedra with two very distinct average Ni-O bond lengths [2,9–13]. Such a lattice modulation attributed CO state is known to be of generic nature in  $\text{RNiO}_3$  nickelates. The ordering persists even in the high temperature regime, well above the antiferromagnetic order temperature

( $T_{\text{N}}$ ) and/or  $T_{\text{MI}}$ . A long-range CO state in  $\text{NdNiO}_3$  along with reported Fermi-surface nesting in nickelates suggests density wave formations, in which the itinerant charge carriers are subjected to strongly coupled degrees of freedom [5,13–15]. Though there are studies on determining the exact ground state of prototype nickelate  $\text{NdNiO}_3$  for which the  $T_{\text{MI}}$  and  $T_{\text{N}}$  points coincide, the immediate next member,  $\text{SmNiO}_3$  (SNO), which is known to be the first nickelate with well separated electronic and magnetic transition temperatures, has not been explored for such ground states. The SNO exhibits a  $T_{\text{N}} \sim 220$  K with antiferromagnetic fluctuations persisting even well beyond the  $T_{\text{N}}$  [16]. Given these properties of SNO and that it exhibits ordered electronic state over a broad temperature range, it is of key importance to understand the ground state of this system.

The  $T_{\text{N}}$  and  $T_{\text{MI}}$  of SNO also are very sensitive to subtle change in the crystal unit cell, just as other nickelates. Its properties can, therefore, be easily tuned via epitaxial strain engineering in thin films and the crystal structure depends on the competition between epitaxial strain and dimensionality [17–19]. In such a scenario, the  $\text{NiO}_6$  octahedral distortion and rotation help to relieve the chemical pressure; although the thin film stoichiometry often favors the defect/impure state to subdue the uncompensated chemical pressure. The SNO is prone to be nonstoichiometric in oxygen content [16–19]. In this phase, the oxygen vacancies can act as defect centers to pin the phase mode of the collective oscillations via building up a substantial impurity potential and lattice imperfection. In this paper, we report investigations on complex THz optical conductivities of epitaxial SNO thin films with different thicknesses. Using the connection of the structural constants with the oxygen content, we show unique control of oxygen nonstoichiometry driven defect center formations such that a CDW type collective mode manifests and depends on the film thickness. These experimental findings

\*dsrana@iiserb.ac.in

pave a way in understanding the evolution of CDW dynamics in the complex CO ground state of  $R\text{NiO}_3$  without the need of chemical perturbation unlike in well-studied manganites.

## II. EXPERIMENT

The epitaxial SNO thin films with thicknesses 25, 65, and 110 nm were deposited on single crystal  $(\text{LaAlO}_3)_{0.3}(\text{Sr}_2\text{TaAlO}_6)_{0.7}$  (LSAT) (100) substrate using pulsed laser deposition technique [20]. The bulk SNO has pseudocubic lattice parameter  $a_{\text{pc}} \sim 3.799 \text{ \AA}$ . The LSAT substrate induces a tensile strain of 1.8% in SNO thin film. The x-ray diffraction (XRD) measurements on the films were performed on a PanAnalytical x-ray diffractometer and dc resistivity measurements were carried out using a physical property measurement system (Quantum Design). The terahertz time domain spectroscopy (THz-TDS) measurements were performed on a photoconductive (LT-GaAs) antenna-based TERA K-8 spectrometer (Menlo Systems GmbH) in the energy range of 0.8–6 meV and the temperature range of 5–300 K.

## III. RESULTS AND DISCUSSIONS

The  $\theta$ - $2\theta$  XRD patterns (Fig. S1) of the Supplemental Material [20] and the reciprocal space mapping (RSM) plots (Fig. S2 [20]) depict a gradual unit cell volume contraction with increasing thickness of SNO films under the cube-on-cube high quality single-crystalline epitaxial growth condition which is further assessed by  $\phi$  scan (Fig. S3 [20]). Analysis of RSM data reveals that the unit cell volume decreases from  $57.31 \text{ \AA}^3$  for 25-nm-thick film to  $56.93 \text{ \AA}^3$  for 110-nm thick film. Given that all the films are coherently strained, a gradual decrease in cell volume may be because of increasing oxygen vacancies with decreasing thickness. This is because the oxygen vacancy will decrease the concentration of  $\text{Ni}^{3+}$  cations which have smaller size than  $\text{Ni}^{2+}$  ion [18,21,22]. This further implies that the thicker films are much more oxygen stoichiometric under the cube by cube coherent growth condition. With increase of SNO layers, a redistribution of the oxygen vacancies can take place and the thicker film will get more stabilized via lowering oxygen vacancies [4,18,19,21,22].

The temperature ( $T$ ) dependence of electrical resistivity ( $\rho$ ) data is useful to approximate the oxygen defects in nickelates. The  $\rho$ - $T$  profiles were acquired in the temperature range of 50–380 K for all the films (Fig. S4 [20]). Analysis of these data suggests a gradual increase in magnetic transition temperature ( $T_N$ ) with an increase in film thickness. The  $T_N$  too is known to be very sensitive to the oxygen stoichiometry as it decreases with higher oxygen vacancies [16]. Combining the information from structural and electrical transport data, it is inferred that the oxygen deficiency/nonstoichiometry increases with decreasing thickness of the SNO films and that the 110-nm film is the most stoichiometric one.

The low energy THz dynamics of these films were investigated in the temperature range of 10–300 K. The THz frequency dependent optical conductivity [ $\sigma(\omega)$ ] spectra of these films at different temperatures are plotted in Fig. 1. A double peaklike structure is clearly evident in 25-nm film.

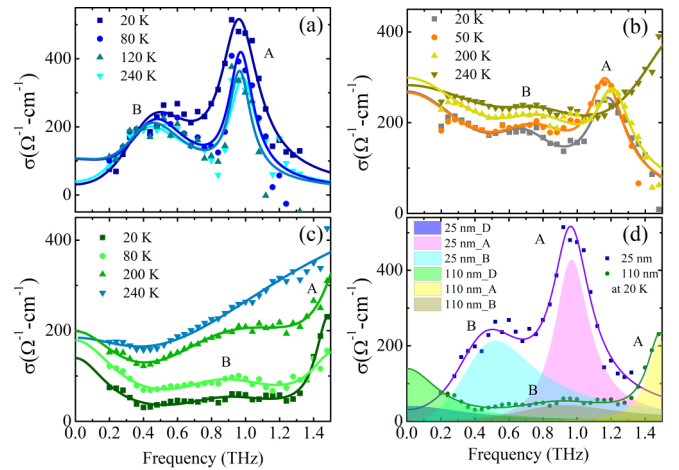


FIG. 1. Frequency dependent optical conductivity ( $\sigma$ ) of SNO/LSAT (100) films of various thicknesses (a) 25 nm, (b) 65 nm, and (c) 110 nm in THz frequency region and at various temperatures. The A and B in each panel indicate two sets of conductivity peaks corresponding to two different resonance frequencies. Solid lines are Drude-Lorentz fit for experimental data. (d) Drude (D) and Lorentz (A and B) contribution in optical conductivity for the films of thicknesses 25 and 110 nm at 20 K.

As the film thickness increases, a systematic variation of peak amplitude is observed. The appearance of peaks in  $\sigma(\omega)$  within such a low energy range of 0.8–6 meV (1 THz–4.13 meV) is a non-Drude-like response which is not an attribute of free carrier dynamics. These peaklike features (at  $\sim 0.5$  and 1.0 THz) manifest at an energy which is about one order of magnitude lower than the energy of the lowest phonon modes in SNO thin film as the Ni-O bending and stretching modes appear at around 35 and 75 meV, respectively [10]. Therefore, such low energy excitation peaks in  $\sigma(\omega)$  are the most probable attributions of a CDW type resonant collective mode. This type of mode has previously been observed in our recent study on  $\text{NdNiO}_3$  epitaxial thin films [5,23–25]. In the case of  $\text{NdNiO}_3$ , the orthorhombic distortion triggers the CDW modes, while in the case of SNO films there is no such dependence on structure. Such investigations were also made on orthorhombic SNO/LSAT (110) film with intermediate thickness  $\sim 75$  nm. In this film too, like the other SNO/LSAT (100) films, doublet resonances were observed [Figs. 2(a) and 2(b)]. The LSAT (110) consists of two different in-plane axes, i.e., (001) and (1-10). In both the directions, the resonance peak occurs at nearly the same energy values. Therefore, it may be surmised that for smaller  $R$ -cation based nickelates, the manifestation of CDW modes is independent of the structure.

The two-peak-like notable feature in  $\sigma(\omega)$ , as explained above, is a rare observation in any class of complex oxides. As seen in Fig. 1(a), the 25-nm film exhibits a strong resonance peak at  $\sim 4$  meV (peak “A”), while there is a comparatively broad hump peak structure in the vicinity of  $\sim 2$  meV (peak “B”). With an increase in SNO film thickness, peak A gradually shifts to a higher energy regime, while peak B becomes relatively broader. For the highest thickness of 110 nm, peak A shifts beyond our experimental range, although a “taillike”

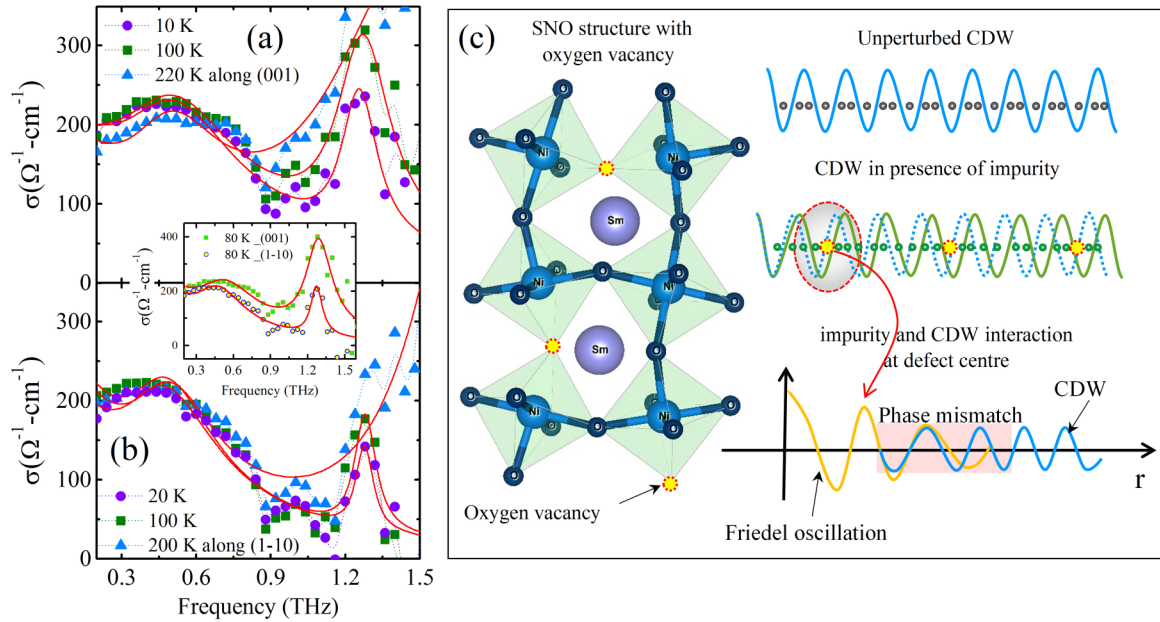


FIG. 2. Panels (a) and (b) depict the frequency dependent optical conductivity of SNO/LSAT (110) film, measured along two different in-plane orthogonal axes. Inset is showing the comparative representation of  $\sigma$  values for the both directions at 80 K. (c) The schematic representation of SNO structure with random oxygen vacancies which act as impurity centers. The unperturbed CDW mode gets entangled with this impurity mediated Friedel oscillation (FO), centered at the impurity, and the phase mismatch between FO and CDW can be witnessed with newly modulated lattice arrangement.

feature seems to appear at lower temperature. Except for the 25-nm film, the strength of peak A gradually diminishes as the temperature approaches the  $T_N$  value. For the 25-nm film, the A peaks remain intact even beyond the corresponding  $T_N$  value, though the peak strength gradually decreases as temperature increases which is a known attribute of the CDW excitation mode. Overall, a film thickness and temperature dependent behavior manifests for these two modes. Though both modes very likely weaken with increase of film thickness, a complete suppression of peak B is observed only for 110-nm film at 240 K [Fig. 1(c)], beyond which only a tail-like feature remains which is most probably associated with the higher energy shifted A peak.

To get a further detailed picture, we have employed the Drude-Lorentz (DL) model to fit the optical response of these thin films (Fig. 1) [20,23,24]. All the data fit well with the DL model; fitted values for 20 and 140 K are listed in Table S1 of the Supplemental Material [20]. With increasing film thickness, an increase in resonant frequency and a decrease of the oscillator strength manifest for both A and B peaks. This emphasizes the weakening of CDW modes upon increase of film thickness. All these observations are very startling and unique for the  $RNiO_3$  family in particular and complex oxides in general. These findings also point towards the complex entanglement between the impurities/lattice imperfections and the CDW modes. According to the CDW model, the collective excitations have two different modes, i.e., phason and amplitudon. The phase fluctuation, i.e., phason mode, is connected with the relative position of the CDW and the lattice. The phason mode can be pinned to the lattice due to any kind of lattice imperfection or impurities and manifests in a relatively lower energy range with respect to the amplitudon mode [23–26]. In

addition, the CDW mode can induce a “bound resonance” as a result of the interaction between impurities and the collective mode itself. In this context, at the absorption edge of any ion, the electronic structure is the most influential factor in determining the single-particle excitations [2]. Such internal deformation mediated resonances are quite perceptible in low energy dynamics, while in the case of high energy dynamics they remain ineffective to contribute significantly [25]. This suggests the efficacy of low energy THz dynamics to elucidate such hidden mechanisms.

In light of the observed structural and dc electrical properties of these SNO thin films, we can conclude that the impurity concentration/lattice imperfection increases with decreasing film thickness. Here, we argue that the observed two excitation modes in the THz energy range are the “pinned” and “bound” states of CDW condensate. It seems that the pinned state (A mode) appears due to both the impurities and commensurability present in our samples; it therefore remains intact in all the films. In contrast, the bound state (B mode) is a very apparent outcome of the interaction between the impurity and the CDW condensate itself. Unlike the pinned mode, the manifestation of the bound mode is strongly dependent on impurity concentration. Therefore, after going through a gradual broadening, it disappears completely in 110-nm film at high temperature, while some signatures of mode A still remain visible at all temperatures (Fig. 1 and Table S1 [20]). The fingerprints of the “strongly pinned” state are dominant in the 25-nm film, which is the highest oxygen nonstoichiometric sample. In this case, both the pinned and bound modes are strongly coupled due to the strong pinning potential around the impurities. Both modes continue to persist even beyond the

magnetic ordering temperature. Also, the films have a vanishingly small Drude spectral weight [Figs. 1(a) and 1(d)] even at the high temperatures. However, the samples with higher oxygen stoichiometry, i.e., with higher thickness, have a substantial Drude contribution. For the 25-nm film, a temperature dependent decrease in mode strength is evident as the contributions of background uncondensed charge carriers is negligibly small.

As the density of oxygen defects decreases, a different picture of the relation of the defect with the modes emerges. Mode A is highly temperature sensitive and so is mode B. As the system approaches its  $T_N$ , mode A shifts towards a higher energy range, while mode B broadens with higher mode strength (Table S1 [20]). At very high temperature and low impurity concentration, mode B completely disappears [Fig. 1(c)]. This confirms the bound nature of mode B, which varies significantly as the system goes through the considerable variation of oxygen defects concentration, concomitant with the variation of the coupling between the impurity and pinned state. In this context, the SNO film on LSAT (110) also exhibits nearly similar behavior as that of the intermediate thick 65-nm SNO film on LSAT (100) substrate. This is so because as the temperature increases, peak A shifts to a higher frequency limit and a prominent signature of peak B persists even at the highest temperature [Figs. 2(a) and 2(b)]. The absence of any anisotropic behavior of these resonance peaks, observed along two different in-plane directions, depicts a dominant role of oxygen vacancies in such CDW type condensation. Only the anisotropic absorption is well evident because of the directional nature of the hybridization of O  $2p$  with Ni  $3d$  orbitals [5].

Based on the data presented and the analysis made above, we present a schematic to visualize the fundamental microscopic mechanism for SNO films in presence of oxygen vacancy states [Fig. 2(c)]. The continuous modulation of CDW is an attribution of the combined effects of the external THz electric field and the pinning centers [27–29]. For the films with larger density of defects, the CDWs are under larger stress and a local amplitude variation of CDW can be expected. The competition between the impurity mediated random force and elasticity of CDW phase defines the overall behavior of the CDW when it interacts with the impurity itself [30–32]. As defined by Friedel, an impurity causes a spatial oscillation of charge density around it [Friedel oscillation (FO)] which interacts with the CDW [27–34]. In such case, the impurity tries to optimize the net charge density around it via locking the phase of FO at the impurity site. Therefore, in the vicinity of impurity, a strong interaction and competition takes place when a relative phase difference between FO and CDW

persists. This phase mismatch further gives rise to the bound states, the energy of which entirely depends on the relative position of the impurities with respect to the CDW [23,24,27–34]. In our present study, with decreasing film thickness, the density of oxygen vacancies and, hence, the defect concentration increases. Our study emphasizes that these defect centers act like an impurity which breaks the translational symmetry in the lattice. The random oxygen defect positions in the SNO lattice array act as a source of the impurity potential which further interacts strongly with the unperturbed CDW to give rise to the bound state in the system [Fig. 2(c)]. These bound states result in an additional low energy excitation mode in the THz optical conductivity. As discussed above, the relative position of the impurity potential with respect to the CDW is a key control for the mode strength and its position. Therefore, a change in density of impurities/defects as a function of SNO film thickness and temperature can provide new control in the modulation of lattice degrees of freedom of CDW at atomic scale.

#### IV. SUMMARY

In this paper, we report a rare observation of pinned and bound modes of the CDW in nickelates or any class of complex perovskites by using low energy attribute of THz spectroscopy. Also, by using samples with different oxygen content/deficiency and, hence, the defect, we have brought out the role of impurities in manifestation of a bound CDW mode and overall control of both the pinned and bound modes. Supported by structural and electrical data, we show that the CDW resonances are strongly dependent on the density of oxygen vacancies and resultant deformed lattice symmetry. This study also brings out a simple yet highly effective method to induce and control dual CDW excitation modes by changing only thickness of the thin film. Besides other applications of this material as CDW conductor, the two resonance modes detected here could be coupled with the THz resonance modes of artificially designed THz materials to control and guide the light adding a different dimension to the area of metamaterials.

#### ACKNOWLEDGMENTS

D.S.R. thanks the Science and Engineering Research Board (SERB), Department of Science and Technology, New Delhi, for financial support under Research Project No. EMR/2016/003598. Financial support from the DST-FIST program is also acknowledged.

- 
- [1] H. Park, A. J. Millis, and C. A. Marianetti, *Phys. Rev. Lett.* **109**, 156402 (2012).  
 [2] U. Staub, G. I. Meijer, F. Fauth, R. Allenspach, J. G. Bednorz, J. Karpinski, S. M. Kazakov, L. Paolasini, and F. d’Acapito, *Phys. Rev. Lett.* **88**, 126402 (2002).

- [3] J.-S. Zhou, J. B. Goodenough, and B. Dabrowski, *Phys. Rev. Lett.* **95**, 127204 (2005).  
 [4] S. Das, V. E. Phanindra, S. S. Philip, and D. S. Rana, *Phys. Rev. B* **96**, 144411 (2017).  
 [5] R. Rana, P. Pandey, V. E. Phanindra, S. S. Prabhu, and D. S. Rana, *Phys. Rev. B* **97**, 045123 (2018).

- [6] T. Mizokawa, D. I. Khomskii, and G. A. Sawatzky, *Phys. Rev. B* **61**, 11263 (2000).
- [7] J. Varignon, M. N. Grisolia, J. Íñiguez, A. Barthélémy, and M. Bibes, *npj Quantum Mater.* **2**, 21 (2017).
- [8] R. J. Green, M. W. Haverkort, and G. A. Sawatzky, *Phys. Rev. B* **94**, 195127 (2016).
- [9] I. I. Mazin, D. I. Khomskii, R. Lengsdorf, J. A. Alonso, W. G. Marshall, R. M. Ibberson, A. Podlesnyak, M. J. Martínez-Lope, and M. M. Abd-Elmeguid, *Phys. Rev. Lett.* **98**, 176406 (2007).
- [10] R. Jaramillo, S. D. Ha, D. M. Silevitch, and S. Ramanathan, *Nat. Phys.* **10**, 304 (2014).
- [11] J. Ruppen, J. Teyssier, I. Ardizzone, O. E. Peil, S. Catalano, M. Gibert, J.-M. Triscone, A. Georges, and D. van der Marel, *Phys. Rev. B* **96**, 045120 (2017).
- [12] J. Ruppen, J. Teyssier, O. E. Peil, S. Catalano, M. Gibert, J. Mravlje, J.-M. Triscone, A. Georges, and D. van der Marel, *Phys. Rev. B* **92**, 155145 (2015).
- [13] S. B. Lee, R. Chen, and L. Balents, *Phys. Rev. Lett.* **106**, 016405 (2011).
- [14] A. Frano, E. Schierle, M. W. Haverkort, Y. Lu, M. Wu, S. Blanco-Canosa, U. Nwankwo, A. V. Boris, P. Wochner, G. Cristiani, H. U. Habermeier, G. Logvenov, V. Hinkov, E. Benckiser, E. Weschke, and B. Keimer, *Phys. Rev. Lett.* **111**, 106804 (2013).
- [15] R. S. Dhaka, T. Das, N. C. Plumb, Z. Ristic, W. Kong, C. E. Matt, N. Xu, K. Dolui, E. Razzoli, M. Medarde, L. Patthey, M. Shi, M. Radović, and J. Mesot, *Phys. Rev. B* **92**, 035127 (2015).
- [16] S. D. Ha, R. Jaramillo, D. M. Silevitch, F. Schoofs, K. Kerman, J. D. Baniecki, and S. Ramanathan, *Phys. Rev. B* **87**, 125150 (2013).
- [17] F. Y. Bruno, S. Valencia, R. Abrudan, Y. Dumont, C. Carrétéro, M. Bibes, and A. Barthélémy, *Appl. Phys. Lett.* **104**, 021920 (2014).
- [18] B. Torriss, M. Chaker, and J. Margot, *Appl. Phys. Lett.* **101**, 091908 (2012).
- [19] B. Torriss, J. Margot, and M. Chaker, *Sci. Rep.* **7**, 40915 (2017).
- [20] See Supplemental Material at <http://link.aps.org/supplemental/10.1103/PhysRevB.102.214403> for experimental details, structural analysis, the resistivity as a function of temperature and THz conductivity fitting model.
- [21] S. D. Ha, G. H. Aydogdu, and S. Ramanathan, *Appl. Phys. Lett.* **98**, 012105 (2011).
- [22] S. Catalano, M. Gibert, V. Bisogni, O. E. Peil, F. He, R. Sutarto, M. Viret, P. Zubko, R. Scherwitzl, A. Georges, G. A. Sawatzky, T. Schmitt, and J.-M. Triscone, *APL Mater.* **2**, 116110 (2014).
- [23] N. Kida and M. Tonouchi, *Phys. Rev. B* **66**, 024401 (2002).
- [24] A. Nucara, P. Maselli, P. Calvani, R. Sopracase, M. Ortolani, G. Gruener, M. C. Guidi, U. Schade, and J. García, *Phys. Rev. Lett.* **101**, 066407 (2008).
- [25] L. Degiorgi and G. Grüner, *Phys. Rev. B* **44**, 7820 (1991).
- [26] L. Degiorgi, B. Alavi, G. Mihály, and G. Grüner, *Phys. Rev. B* **44**, 7808 (1991).
- [27] D. Feinberg and J. Friedel, *J. Phys.* **49**, 485 (1988).
- [28] L. Degiorgi and G. Grüner, *Europhys. Lett.* **16**, 97 (1991).
- [29] D. Reagor and G. Gruner, *Phys. Rev. Lett.* **56**, 659 (1986).
- [30] H. Fukuyama and P. A. Lee, *Phys. Rev. B* **17**, 535 (1978).
- [31] I. Tütto and A. Zawadowski, *Phys. Rev. B* **32**, 2449 (1985).
- [32] A. I. Larkin, *Zh. E'ksp. Teor. Fiz.* **105**, 1793 (1994) [*JETP* **78**, 971 (1994)].
- [33] I. Tütto and A. Zawadowski, *Phys. Rev. Lett.* **60**, 1442 (1988).
- [34] J.-P. Pouget, *C. R. Phys.* **17**, 332 (2016).